Journal of Solid State Chemistry 183 (2010) 988–993

Contents lists available at ScienceDirect

Journal of Solid State Chemistry

journal homepage: www.elsevier.com/locate/jssc

Electrochemical Li insertion studies on $WNb_{12}O_{33}$—A shear ReO_3 type structure

D. Saritha [a], V. Pralong [b], U.V. Varadaraju [a,*], B. Raveau [b]

[a] Department of Chemistry, Indian Institute of Technology Madras, Chennai 600036, India
[b] Laboratoire de Cristallographie et Sciences des Matériaux, ENSICAEN, Université de Caen, CNRS, 6 Bd Maréchal Juin, F-14050 Caen 4, France

ARTICLE INFO

Article history:
Received 14 January 2010
Received in revised form
26 February 2010
Accepted 1 March 2010
Available online 7 March 2010

Keywords:
Shear ReO_3
$WNb_{12}O_{33}$
Li insertion
Electrochemical properties

ABSTRACT

Electrochemical lithium insertion studies on $WNb_{12}O_{33}$ synthesized by solid state reaction (SSR) are carried out in the voltage range 1.0–3.2 V. During first discharge 15.6 Li are inserted with a specific capacity of 221 mAh/g. $WNb_{12}O_{33}$ is also synthesized by sol–gel (SG) technique with a view to enhance the rate capability and cycling properties. The SSR and SG samples are characterized by powder X-ray diffraction (XRD), scanning electron microscopy (SEM) and galvanostatic cycling. Electrochemical cycling performance of SG samples is superior to that of the SSR sample at high 'C' rates. The sample synthesized by SG method exhibits high specific capacity of 142 mAh/g after 20 cycles at 20C rate.

1. Introduction

The structure of ReO_3 consists of ReO_6 octahedra connected via common corners, extending along the three crystallographic directions that leaves space for foreign ions to occupy (vacant sites) [1]. These vacant sites are connected along the three crystallographic directions rendering the structure attractive as a host to lithium ions [2–4]. However, the extent and rate of lithium insertion depends not only on structural features but also on the particle size, shape and morphology [5]. Li insertion into ReO_3 structure leads to structural distortion; the octahedra are twisted about their shared corners and the stacking changes from $\frac{3}{4}$ CCP to complete HCP [6]. In the case of 'shear ReO_3' structure some of the octahedra are edge shared and hence the path of Li is limited to one direction i.e., along the *c*-axis. Crystallographic shear in ReO_3 structure stabilizes the structure even after lithium insertion [7]. Cava et al. found that in many shear ReO_3 structures small crystallographic shear is necessary to stabilize the host structure during lithium insertion. The Nb_2O_5–WO_3 binary phase diagram has drawn considerable attention due to the presence of stable niobium–tungsten mixed phases (Wadsley–Roth phases) of different structural types [8]. Wadsley–Roth phases are chemically related compounds with different extents of crystallographic shear. 'Shear ReO_3' is one of the structure types adopted by them. Tungsten–vanadium oxides forming this type of structural framework were proposed as probable candidates for electrodes in secondary lithium batteries [9]. Recently, electrochemical lithium insertion studies in $W_4Nb_{26}O_{77}$, $P_8W_{12}O_{52}$, $W_3Nb_{14}O_{44}$ and PNb_9O_{25} with ReO_3 structure type have been carried out [10–13]. Lithium insertion studies on Nb_2O_5 based Wadsley–Roth phases show that a large number of Li ions can be inserted without any major structural change [9,14].

$WNb_{12}O_{33}$ belongs to 'shear ReO_3' structure type [8]. The structure of $WNb_{12}O_{33}$ is shown in Fig. 1. The structure can be described as ReO_3 type blocks of NbO_6 octahedra. Each of the blocks is formed by three corner connected octahedra along *a*-axis and four corner connected octahedra along *b*-axis and extend infinitely along the *c*-axis. The blocks are connected to each other by edge sharing of the octahedra resulting in the shear structure. W atoms are present in tetrahedral coordination and are ordered [8]. The high oxidation state of the elements involved in the oxide framework presents the possibility of facile reduction of the metal ions and thus, facilitates the insertion of Li. In the present study, we have carried out Li insertion studies on $WNb_{12}O_{33}$. The electrochemical Li insertion properties and rate capabilities of $WNb_{12}O_{33}$ synthesized by SSR and SG methods are studied and compared.

2. Experimental

2.1. Synthesis

$WNb_{12}O_{33}$ was synthesized by SSR and SG methods for comparing the effect of particle size on the electrochemical performance. The starting materials used were high pure W

* Corresponding author. Tel.: +91 44 22574215.
E-mail address: varada@iitm.ac.in (U.V. Varadaraju).

0022-4596/$ - see front matter © 2010 Elsevier Inc. All rights reserved.
doi:10.1016/j.jssc.2010.03.003

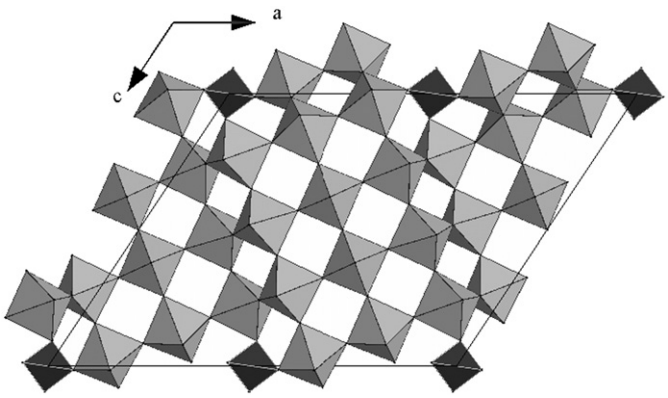

Fig. 1. Schematic representation of the crystal structure of $WNb_{12}O_{33}$.

(Cerac, 99.9%), WO_3 (Alfa, 99.7%), Nb_2O_5 (Alfa, 99.9%), $NbCl_5$ (Aldrich, 99.9%), H_2O_2 (Merck, 30%) and aq. NH_4OH (Merck, 25%).

2.2. Solid state reaction (SSR)

Stoichiometric amounts of WO_3 and Nb_2O_5 were ground under acetone and the powder was pressed into 10 mm diameter pellets. The pellets were placed in an alumina crucible and covered with the powder of the same composition. The crucible was then placed in a furnace and slowly heated to 1150 °C for 45 h. After the heat treatment, the product was quenched to room temperature [10]. The process was repeated until a single phase is obtained.

2.3. Sol–gel synthesis (SG)

The $WNb_{12}O_{33}$ phase is also synthesized by SG method in order to overcome the disadvantages of SSR method i.e., large particle size of the product, sample inhomogeneity and volatilization of W. In the SG method W powder was dissolved in a mixture of 40 ml of 30% H_2O_2 and 4 ml of deionized water. The mixture was stirred until a clear solution results (A). The reaction being exothermic is carried out in an ice bath. $NbCl_5$ powder was dissolved in 10 ml of ethanol and 20 ml of 30% H_2O_2 in an ice bath yielding a transparent yellow solution (B). Aqueous citric acid solution was added to the mixed solution of A and B under constant stirring to obtain a sol. The ratio of citric acid:metal ions is 3:1. The pH of the solution was adjusted to 7 and ethylene glycol solution was added to this for gel formation. After stirring for 5 h, a transparent yellow gel was obtained. The gel was decomposed by heating at 700 °C for 24 h. The decomposed product is further heated at 1150 °C for 5 h for phase formation.

2.4. Characterization

X-ray powder diffraction patterns were recorded in the 2θ range 5–120° using a Philips X'pert diffractometer with Bragg-Brentano geometry using Cu$K\alpha$ source. Ex-situ XRD characterization was carried out by Rigaku miniflex X-ray diffractometer in the 2θ range 10–70° by covering the electrodes with Mylar film. The morphology of the samples synthesized by SSR and SG methods was established by a scanning electron microscope (SEM, FEI Quanta 200). Galvanostatic charge/discharge cycling studies were carried out by using an Arbin battery cycling unit (Arbin Instruments, BT 2000, USA).

Electrochemical lithium insertion/extraction studies were performed in Swagelok type cells. Electrodes were fabricated by spreading a mixture of 70 wt% active material and 20 wt% acetylene black (Denka Singapore Pvt. Ltd.) with 10 wt% PVDF in *N*-methyl pyrrolidine (NMP) on a stainless steel foil. Swagelok cell assembly was carried out in an argon filled glove box (mBraun, 120G, and Germany). Teklon (Anatek, USA) was used as the separator and Lithium metal (Aldrich, 99.9%) as counter electrode. The electrolyte used was 1 M $LiPF_6$ in 1:1EC+DMC (Chile Industries Ltd., Korea).

3. Results and discussion

3.1. Phase formation and characterization

Rietveld refinement of the XRD patterns (Fig. 2) of $WNb_{12}O_{33}$ prepared by both SSR method (referred to as 'SSR samples') and SG method (referred to as 'SG samples') show sharp peaks indicating the formation of a crystalline phase. $WNb_{12}O_{33}$ phase crystallizes in a monoclinic unit cell with space group C2 with two formula units (f.u.) per unit cell ($Z=2$). The observed, calculated and difference patterns of $WNb_{12}O_{33}$ prepared by both SSR and SG methods are given in Fig. 2. The refined unit cell parameters and obtained R_{wp}, Bragg R and R_f factors are given in Table 1; the values are in good agreement with those reported in the literature [8]. Fig. 3 presents the SEM pictures of samples prepared by both SSR and SG methods. The particle size for the SSR sample is in the range 1–5 μm, whereas that of the SG sample is in the range 500–600 nm.

3.2. Chemical Li insertion

Chemical insertion was carried out at room temperature using 1.6 M solution of *n*-butyl-lithium (*n*-BuLi) in hexane (equivalent to a potential of 1 V vs. Li/Li^+). The powder was kept in the *n*-BuLi solution for 4 days under constant stirring at RT at the end of which the solution was decanted and the powder was washed several times with hexane, dried under vacuum for several hours and kept in an argon-filled dry box. For the estimation of the amount of inserted lithium, the compound was dissolved in 5%HF solution and the Li was estimated by ICP analysis. Indeed, the fully reduced phase contains 10 moles of lithium/f.u. from the ICP

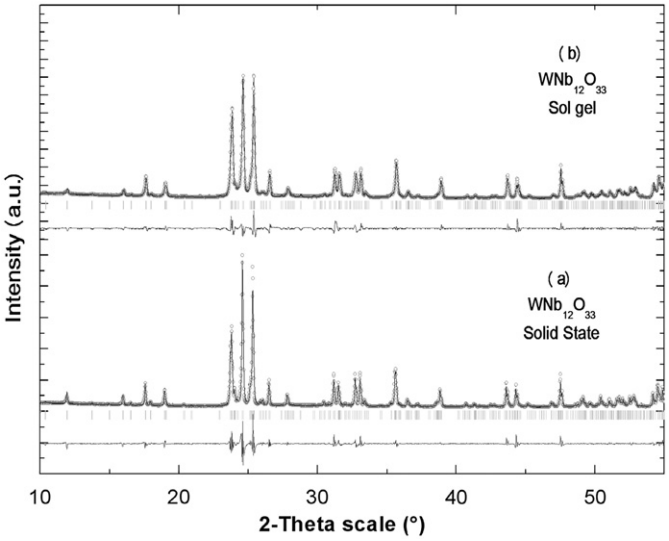

Fig. 2. Powder X-ray diffraction patterns of $WNb_{12}O_{33}$ synthesized by (a) solid state reaction and (b) sol–gel methods.

Table 1
Cell parameter and volumes for the two as prepared $WNb_{12}O_{33}$ phases.

Compositions	$WNb_{12}O_{33}$ by SSR	$Li_xWNb_{12}O_{33}$ by SSR	$WNb_{12}O_{33}$ by SG	$Li_xWNb_{12}O_{33}$ by SG
Space group	*C*2	C2	C2	*C*2
a (Å)	22.31	21.95(3)	22.26(2)	21.92(7)
b (Å)	3.827	4.12(9)	3.82(2)	4.12(2)
c (Å)	17.75	17.6(7)	17.72(4)	17.6(6)
β (deg.)	123.34(2)	123.1 (6)	123.31(4)	122.9 (2)
Cell volume (Å^3)	1266.08	1333.3	1259.8(2)	1334.5
χ^2 (%)	10.5	–	14.1	–
R_{wp}	11.7	–	14.0	–
R_b (%)	1.28	–	1.59	–
R_f (%)	1.04	–	1.07	–

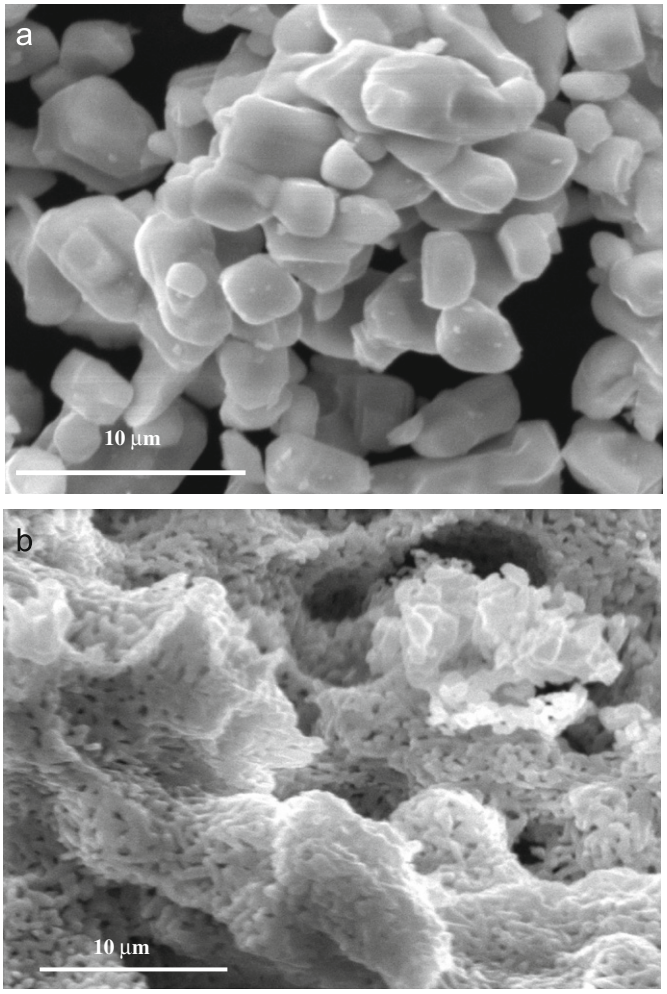

Fig. 3. SEM picture of $WNb_{12}O_{33}$ (a) synthesized by solid state reaction and (b) synthesized by sol–gel method.

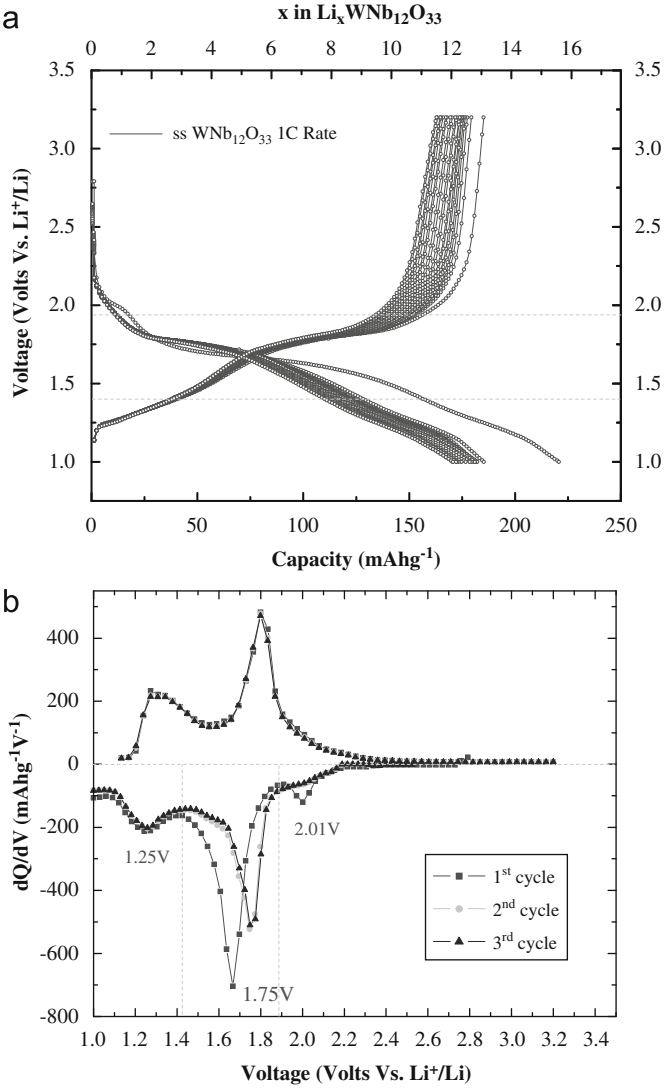

Fig. 4. (a) Charge–discharge cycling curves of $WNb_{12}O_{33}$ prepared by solid state reaction for a galvanic rate of 1C; (b) corresponding differential capacity plots (dQ/d*V*).

analysis (PerkinElmer DV 5300). Thus, the chemical insertion studies indicate that 10 Li can be inserted in the $WNb_{12}O_{33}$ phase which is in excellent agreement with earlier reports [13–14].

3.3. *Electrochemical lithium insertion*

The electrochemical lithium insertion/extraction studies on $WNb_{12}O_{33}$ were performed with a rate of 1C (reaction of one Li in one hour) in the potential window of 1.0–3.2 V. The charge/discharge curves for 20 cycles and the differential capacity plots for the first three cycles are shown in Fig. 4(a) and (b), respectively, for the SSR samples. During the first discharge, a capacity 221 mAh/g was observed. This corresponds to reaction of 15.6 Li per f.u. of $WNb_{12}O_{33}$, equivalent to 1.2 Li per metal atom. An irreversible capacity loss of 3 Li is observed in first charge–discharge cycle, leading to a reversible capacity of 12.6 Li

(185 mAh/g). The first discharge consists of three distinct plateaus at around 2.01, 1.75, 1.25 V vs. Li^+/Li. The three plateaus can be clearly seen from the differential capacity plots (Fig. 4(b)). The potentials corresponding to the three plateaus are in good agreement with those reported for $W_9Nb_8O_{47}$, $(PO_2)_4(WO_3)_{2m}$ and PNb_9O_{25} [13,15,16] and correspond to the reduction of W^{+6} to W^{+5}, Nb^{+5}/Nb^{+4} and Nb^{+4}/Nb^{+3}, respectively. Thus, of the reaction of 15.6 Li observed in the first discharge, 13 Li can be attributed to the reduction of one atom of W^{6+} to W^{5+} and 12 atoms of Nb^{5+} to Nb^{4+}. The remaining is attributed to partial reduction of Nb^{4+} to Nb^{3+}. The area under the curve corresponding to 1.75 V in the differential capacity plot (Fig. 4(b)) is large compared to that corresponding to 1.25 V. The arguments are in line with the earlier reports [13,15,16]

A discussion on the possible sites in the lattice occupied by inserted Li is in order. According to Cava et al. [14], in $WNb_{12}O_{33}$ three different cavity types are identified per formula unit viz., two Type II, four Type III and one Type VI are available for Li insertion (14 cavities per unit cell) [14] (Fig. 5). The Type II cavity formed by a single capped ReO_3 type cuboctahedron can accommodate at least one Li. On the other hand, the Type III cavity, bicapped with a tetrahedral metal atom, has two available sites for Li. Type VI cavity cannot accommodate Li atom [7]. The metal–oxygen distances play an important role in determining the amount of Li accommodated in these structures [17]. For example, in $(Mo_{0.3}V_{0.7})_2O_5$ having the same structure as V_2O_5 (Type III cavity), the metal–oxygen bond length decreases from 2.81 to 2.54 Å due to the Mo doping and as a result the size of Type III cavity increases and accommodates more than 2 Li at room temperature [18]. $WV_2O_{7.5}$ which has Type II cavities in the structure can accommodate 2 lithium atoms instead of one lithium atom [14]. It is also found that in VNb_9O_{25}, Li can be accommodated in Type VI cavity [14]. Based on these earlier observations, the intercalation of 15 Li per formula unit, in the present case, can be rationalized. Since there are 7 possible cavities in the structure (two Type II, four Type III and one Type VI), it is possible to accommodate at least 14 Li per f.u. assuming two Li atoms can occupy each cavity. The remaining 1.6 Li can be accommodated in the Type III cavity as mentioned earlier [18].

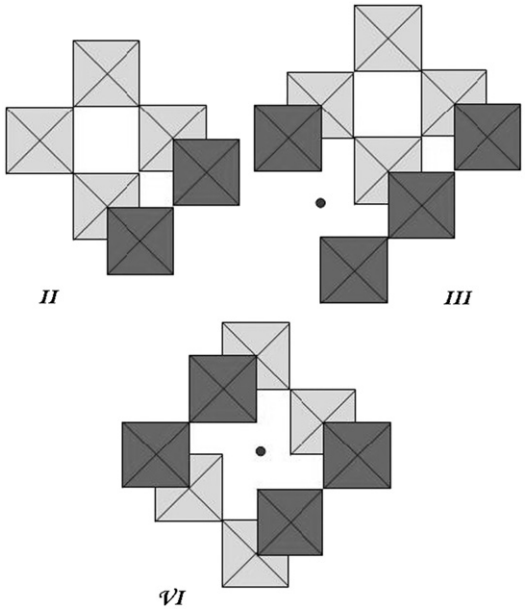

Fig. 5. Cavity types of available sites present in $WNb_{12}O_{33}$ described by Cava et al [9].

Structural changes in the framework of the host as lithium insertion proceeded were followed by ex-situ X-ray diffraction technique. The electrodes were covered with Mylar film and ex-situ XRD patterns were recorded. The powder XRD patterns of Li inserted phase (first discharge) (Fig. 6(b)) is similar to that of the parent phase (Fig. 6(a)), barring the expected broadening of the peaks due to the room temperature insertion reaction. Shifts in the peak positions are observed as a result of Li insertion. The structure remains intact after extraction (first cycle) (Fig. 6(c)) as evidenced from the similarity of the XRD patterns of the pristine, Li inserted and extracted phases. The calculated lattice parameters after Li insertion are given in Table 1. In the lithiated phase, the '*a*' and '*c*' lattice parameter decreases and the '*b*' parameter increases vis-á-vis the parent phase. Such anisotropic behavior of change in lattice parameters upon Li insertion is reported in the literature [14]. The XRD pattern of the electrode after 20 cycles remains the same (not shown). The ex-situ XRD results confirm that the structure of $WNb_{12}O_{13}$ is amenable for reversible Li insertion.

3.4. Comparative studies

To overcome the disadvantages of inhomogeneity, tungsten volatilization, and large particle size associated with SSR synthesis, and in order to improve the charge/discharge rate capability, we synthesized $WNb_{12}O_{33}$ by SG method and compared the electrochemical properties with those of the sample synthesized by SSR. Reduced particle size is one of the effective ways to

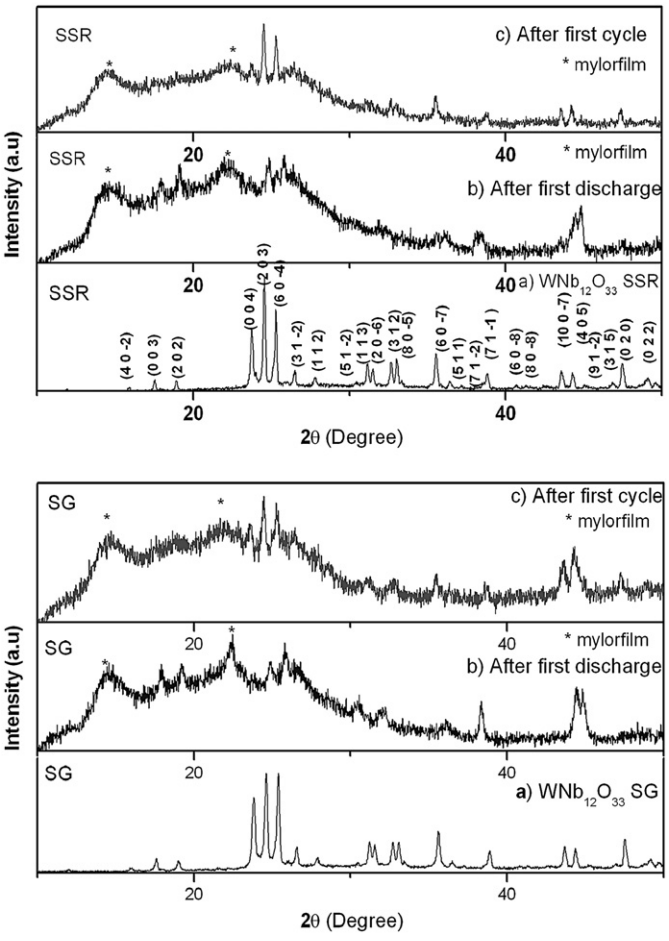

Fig. 6. Ex-situ XRD patterns of $WNb_{12}O_{33}$ prepared by both SSR and SG methods (a) before discharge, (b) after discharge to 1 V and (c) after first cycle.

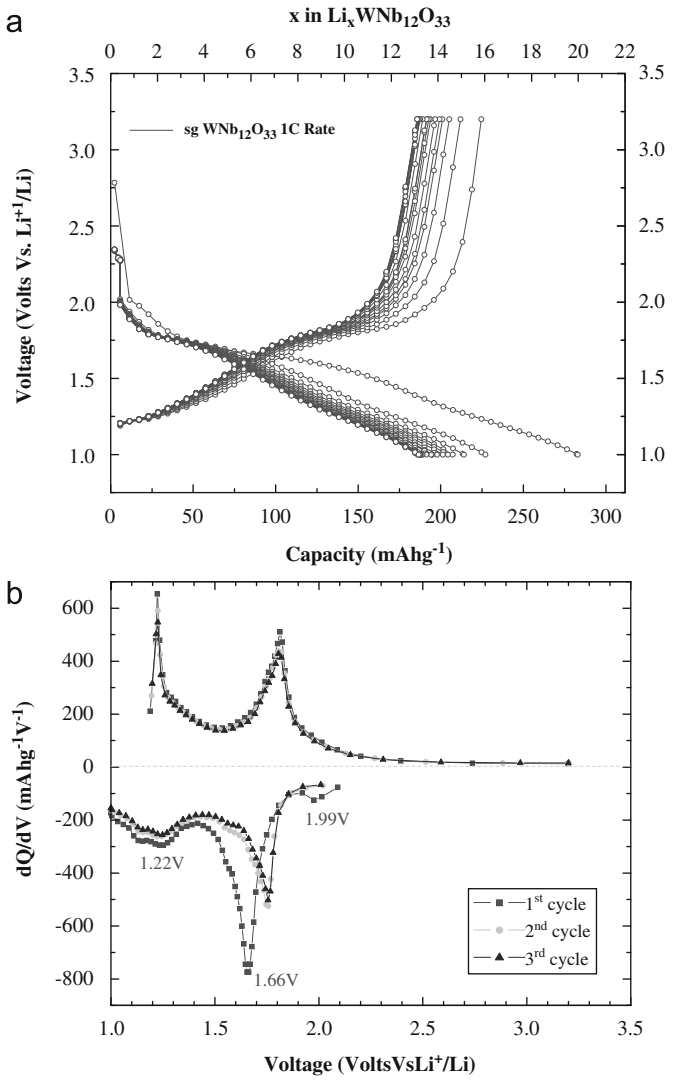

Fig. 7. (a) Charge–discharge curves of sol–gel prepared $WNb_{12}O_{33}$ at a galvanic rate of 1C; (b) corresponding differential capacity plots (dQ/d*V*).

improve the rate performance. Shorter diffusion length and high surface area of the smaller particles improves the lithium insertion kinetics leading to high rate performance. The galvanostatic charge/discharge curves and the corresponding differential capacity plots of the sample synthesized by SG method are shown in Fig. 7(a) and (b). The discharge capacity is 282 mAh/g corresponding to the insertion of 19.2 Li. The first charge capacity is 226 mAh/g corresponding to the extraction of 15.4 Li. The plateaus observed in the case of the SG sample correspond very well to those observed in the case of SSR sample. However, the capacity observed in the case of SG sample (226 mAh/g) is higher compared to that of the SSR sample (185 mAh/g). This can be attributed to the reduction, further, of Nb^{+4} to Nb^{+3}. West et al. have observed that it is possible to intercalate 3 Li atoms per V_2O_5 f.u. electrochemically at 100 °C whereas, only one Li could be intercalated at room temperature. The V_2O_5 structure has bicapped cuboctahedron cavities (Type III). In these cavities two opposite square faces are capped with oxygen providing two additional square pyramidal sites with the capping oxygens at the apices. The inserted Li atoms reside in square pyramidal sites coordinated by 5 oxygen atoms [19]. The temperature dependence of the insertion suggests that it is possible to increase the extent of Li insertion by facilitating the diffusion. Li diffusion can also be facilitated by reducing the particle size as is observed

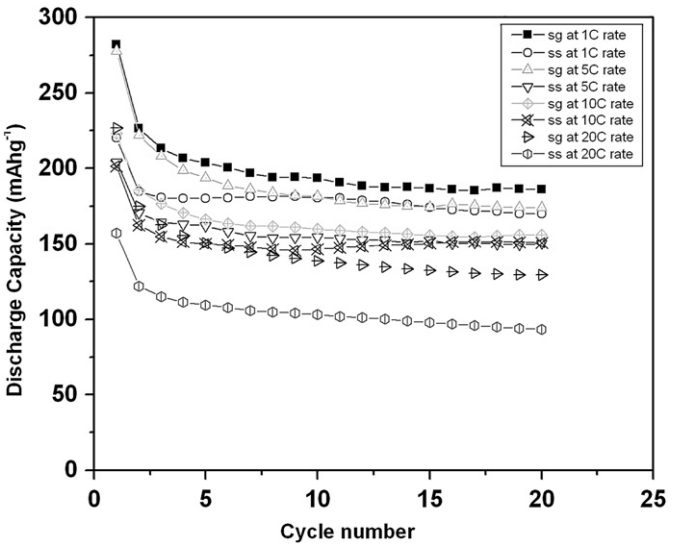

Fig. 8. Comparison of the capacity versus cycle number for the two $WNb_{12}O_{33}$ samples at various *C*/*n* rates.

in the present case of the sample synthesized by SG method. 19.2 Li are inserted in the first discharge vis-å-vis 15.6 Li in the SSR sample. The extra Li (4.2) reacted in the case of SG sample can be accommodated in all the four Type III cavities. The ex-situ XRD patterns of the electrodes after first discharge and first cycle reveal that the structural integrity is retained (Fig. 6).

Fig. 8 shows the comparison of electrochemical cycling performance of $WNb_{12}O_{33}$ prepared by SG and SSR methods at charge/discharge rates of 1–20C. At 1C rate, after the first cycle, the SG sample shows higher capacity compared to that of the SSR sample. In addition, the improved Li insertion kinetics in the smaller particles with higher surface area of the SG samples result in higher capacity as mentioned above. Both SSR and SG samples show comparable capacities at low rates of charge/discharge after 20 cycles. Low rates provide sufficient time for Li to diffuse even in the SSR sample. However, at higher C rates, the capacity retention of the SG sample is superior. At a discharge rate of 20C, a high capacity of 142 mAh/g is obtained for the SG sample, even after 20 cycles whereas, the corresponding value for the SSR sample is 107 mAh/g. The $WNb_{12}O_{33}$ prepared by SG method shows lower capacity fading at high C rates when compared with that of the SSR sample.

4. Conclusion

In the present study, $WNb_{12}O_{33}$ phase, which crystallizes with the shear ReO_3 structure, is synthesized by both SSR and SG methods. Electrochemical Li insertion/extraction studies show that $WNb_{12}O_{33}$ is a good host for insertion/extraction reactions as the structure can reversibly incorporate a relatively large amount of Li atoms in the voltage window 3.2–1.0 V, retaining the structural integrity. The SG synthesized samples show better electrochemical performance when compared to the SSR samples in terms of higher capacity, higher rate capability and superior capacity retention. The studies demonstrate the high 'C' rate capability of $WNb_{12}O_{33}$ in the pseudo-nano regime.

Acknowledgements

This work is carried out in the framework of LAFICS and the financial support from IFCPAR (Indo-French Centre for the

Promotion of Advanced Research/Centre Franco-Indian Pour la Promotion de la Recherché Advance) is gratefully acknowledged.

References

[1] D.W. Murphy, Solid State Ionics 18-19 (1986) 847–851.
[2] L. Permer, J. Solid State Chem. 97 (1992) 105–114.
[3] M. HibinoW. Han, T. Kudo, Solid State Ionics 135 (2000) 61–69.
[4] M. Montemayor, A. Mendez, A. Martinez-de la Cruz, A.F. Fuentes, L.M. Torres-Martinez, J. Mater. Chem. 8 (1998) 1805–1807.
[5] Kiyoshi Kanamura, Shohei Koizumi, Kaoru Dokko, Mater. Sci. 43 (2008) 2138–2142.
[6] R.J. Cava, A. Santoro, D.W. Murphy, S. Zahurak, R.S. Roth, J. Solid State Chem. 42 (1982) 251–262.
[7] R.J. Cava, A. Santoro, D.W. Murphy, S. Zahurak, R.S. Roth, Solid State Ionics 5 (1981) 323–326.
[8] J.G. Allpress, A.D. Wadsley, Issue Series Title: J. Solid State Chem. 1 (1969) 28–38.
[9] R.J. Cava, D.W. Murphy, S.M. Zahurak, J. Electrochem. Soc. 130 (1983) 243–245.
[10] A.F. Fuentes, E. Briones Garza, A. Martinez-de la Cruz, L.M. Torres-Martinez, Solid state Ionics 93 (1997) 245–253.
[11] A. Martínez-de la Cruz, F.E. Longoria Rodríguez, J. Ibarra Rodríguez, Solid State Ionics 176 (2005) 2625–2630.
[12] A.F. Fuentes, A. Martinez-de la Cruz, L.M. Torres-Martinez, Solid State Ionics 92 (1996) 103–111.
[13] S. Patoux, M. Dolle, G. Rousse, C. Masquelier, J. Electrochem. Soc. 149 (4) (2002) A391–A400.
[14] R.J. Cava, D.W. Murphy, S.M. Zahurak, J. Electrochem. Soc. 30 (1983) 2345–2351.
[15] A. Martinez-de la cruz, I. Ramirez, L.C. Gonzalez, Mater. Res. Bull. 38 (2003) 525–531.
[16] A. Martinez-de la cruz, F.E. Rodriguez, T. GonZalez, L.M. Torres-Martinez, Electrochim. Acta 52 (2007) 6490–6495.
[17] G. Pistolia, J.Power Sources 9 (1983) 307–320.
[18] M. Pasquali, G. Pistolia, F. Rodante, J. Power Sources 7 (1982) 145–152.
[19] K. West, B. Zachau-Christiansen, T. Jacobsen, S. Skaarup, Solid State Ionics 76 (1995) 15–21.